Two-dimensional electron momentum spectra of argon ionized by short intense lasers: Comparison of theory with experiment

Toru Morishita,[1,2] Zhangjin Chen,[2] Shinichi Watanabe,[1] and C. D. Lin[2]

[1]*Department of Applied Physics and Chemistry, University of Electro-Communications, 1-5-1 Chofu-ga-oka, Chofu-shi, Tokyo 182-8585, Japan*

[2]*Department of Physics, Kansas State University, Manhattan, Kansas 66506, USA*

We studied the two-dimensional electron momentum spectra of Ar by femtosecond intense laser pulses with mean wavelength from 400 nm to 800 nm, to compare with experimental results of Maharjan *et al.* [J. Phys. B **39**, 1955 (2006)]. At the higher intensities we found that the effects of ground-state depletion and laser-focus volume are very important such that the peak laser field strength is not reached in experiment. The ubiquitous fanlike stripes in the low-energy electron momentum spectra and the evidence of Freeman resonances in the experimental data are well reproduced in the theoretical calculations. We emphasize that depletion of the initial state should be carefully evaluated for ionization of atoms in the tunneling region.

PACS number(s): 32.80.Rm, 32.80.Fb, 42.50.Hz

I. INTRODUCTION

When atoms are exposed to an intense short laser pulse, the ejection of the electrons can be conveniently distinguished into two regions, depending on the laser intensity and the wavelength, by using the Keldysh parameter [1], $\gamma = \sqrt{I_p/(2U_p)}$, where I_p is the ionization potential of the target atom and U_p is the ponderomotive energy. If $\gamma > 1$—i.e., in the multiphoton ionization regime—the liberation of the electron is understood to proceed through the absorption of many photons, leading to the above-threshold ionization (ATI) peaks in the electron spectra. In this region, the energy spectra and the angular distributions are often dominated by complex structures due to the Freeman resonances [2]. Many experimental electron spectra, in particular of rare gas atoms, have been carefully studied and examined theoretically [3–6]. At higher laser intensities, when $\gamma < 1$, tunneling ionization becomes dominant. The small-γ region has been investigated experimentally in recent years [7–13] but the interpretation of the data appears to be somewhat confusing so far.

In an early experiment, Moshammer *et al.* [7] reported that the momentum spectrum of Ne$^+$ along the direction of laser polarization shows a minimum at zero momentum when Ne is ionized using a 25-fs 800-nm laser with peak intensity of 1.0×10^{15} W/cm^2. This was considered as a surprise since the tunneling theory predicts a maximum at zero momentum. Rescattering was suggested as the reason for the minimum which was in agreement with an earlier classical calculation [8]. Dimitriou *et al.* [9] showed that the effect is caused by the influence of the Coulomb force on the outgoing electrons rather than by the rescattering. Faisal and Schlegel [10] showed that the minimum can be expected by discrete photon absorption even in the tunneling region. Further experimental results [11–13] show that this minimum occurs for Ne and He, but not for Ar, suggesting that the structure of the target atom plays a role.

For single ionization, recoil-ion momentum images and electron momentum images in principle give the same information. However, the latter offers higher resolution. Thus more recent studies of single ionization of rare gas atoms determined the two-dimensional electron momentum spectra. Initial data by Rudenko *et al.* [11] show complex structures in the low-electron energy region. Arbó *et al.* [14] suggested that the structures are not from resonances but from the diffraction of the ejected electrons by the Coulomb field of the core ion. By comparing the two-dimensional electron momentum spectra calculated using the strong field approximation (SFA) and from solving the time-dependent Schrödinger equation, Wickenhauser *et al.* [15] showed that the low-energy momentum distributions calculated using the two models differ significantly. By solving the time-dependent Schrödinger equation with the same Ar model potential but artificially turning off the Coulomb potential tails, Chen *et al.* [16] concluded that the long-range Coulomb potential modifies the low-energy electron spectra significantly. With the Coulomb potential, the two-dimensional electron momentum spectra exhibit fanlike structures which emanate radially from the center, while the removal of the long-range Coulomb potential results in spectra which tend to lie perpendicular to the laser polarization direction, in agreement with the results from the SFA. Chen *et al.* [16] further showed that the fanlike structures depend only on the orbital angular momentum of the initial state and the minimum number of photons needed to ionize the atom. Interestingly, the fanlike structure does not depend on the nature of the atoms except their initial state angular momentum and binding energy.

Existing theoretical electron spectra for ionization in the tunneling region have not been directly compared to measurements. It is well known that the ATI electron spectra depend sensitively on the laser intensities. Experimentally measured spectra can be compared to theoretical calculations only after the latter have been integrated over the laser-focus volume of the gas jet. This means that the electron spectra have to be calculated at many intensities using very small incremental steps. In this paper we carried out such studies in view of the recent detailed high-resolution electron spectra reported by Maharjan *et al.* [12].
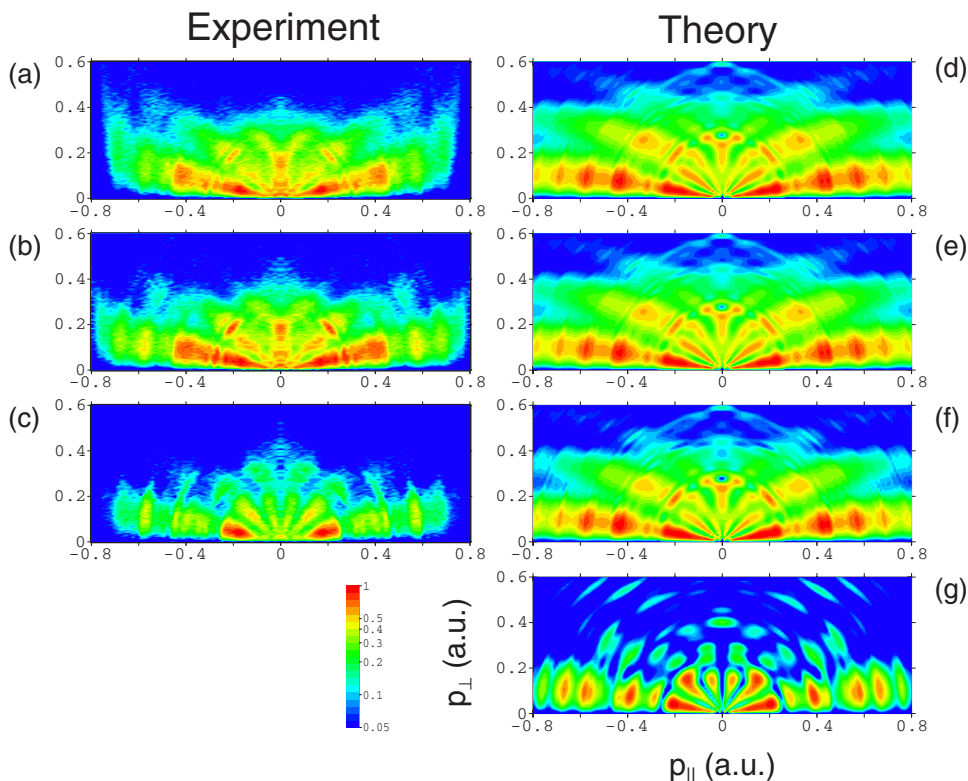
FIG. 1. (Color online) Comparison of theoretical and experimental electron momentum distributions of Ar by a 640-nm 40-fs laser pulse with peak intensities [(a) and (d)] 8.2×10^{14} W/cm^2, [(b) and (e)] 7.08×10^{14} W/cm^2, [(c) and (f)] 3.94×10^{14} W/cm^2, and (g) 1.0×10^{14} W/cm^2.

II. ANALYSIS OF THE THEORETICAL AND EXPERIMENTAL EJECTED ELECTRON MOMENTUM SPECTRA

In Maharjan *et al.* [12] the two-dimensional electron momentum spectra from single ionization of Ar atoms have been measured by laser pulses of durations of 25–50 fs and mean wavelengths from 40 to 800 nm, for different laser intensities. In Fig. 1 the left column shows the spectral images from their measurements for 640-nm 40-fs laser pulses with peak intensities of (a) 8.2×10^{14} W/cm^2, (b) 7.08×10^{14} W/cm^2, and (c) 3.94×10^{14} W/cm^2. Immediately there are two obvious questions. First, why are the spectra in (a) and (b) so similar? In fact, even (c) appears to be rather close to (a) and (b). Second, why do the electron spectra show so many structures? In particular, why are radial stripes fanning out from the center clearly seen in all the frames? Theoretical calculations from solving the time-dependent Schrödinger equation show that the electron spectra change rapidly with the peak laser intensities; thus, one intuitively expects that the electron spectra become featureless after integration over the laser-focus volume. In this paper we investigated how the volume integration affects the two-dimensional electron momentum spectra.

We treat the Ar atom in the single active electron approximation. The ejected electron momentum spectra for each fixed peak intensity are calculated from solving the time-dependent Schrödinger equation. The computational methods are summarized in the Appendix. In the tunneling ionization region, the ionization rate is quite large; thus, the depletion effect should be considered. In Fig. 2 we show the time dependence of the ground-state populations of Ar in the field of a 640-nm 10-fs [full width at half maximum (FWHM)]

laser pulse, at different peak intensities. Here we assume that the temporal dependence of the laser's electric field is cosine squared; see Eq. (A2). At the two higher intensities, clearly the depletion is such that the atom never experiences the peak field strength since ionization is already nearly complete before the peak field is reached. Thus the peak laser intensity and the actual pulse durations are irrelevant. For such a pulse, the laser-focus volume clearly would play an important role as well.

Let us discuss the laser focus volume effect. We assume that the gas volume is larger than the laser-focus volume. Thus the ejected electron signals are the sum of electrons ionized from atoms within the interaction volume. The ionization yields should be weighted by the volume element at each intensity. For a peak intensity I_0, the electron signal with momentum **p** is given by

$$S(\mathbf{p}, I_0) = D \int_0^{I_0} P_I(\mathbf{p}) \left(-\frac{\partial V}{\partial I} \right) dI, \quad (1)$$

where D denotes the density of the target atoms in the interaction volume, $P_I(\mathbf{p})$ is the ionization probability for a particular intensity of I, and $\left(-\frac{\partial V}{\partial I} \right) dI$ represents the volume element for having the intensity between I and $I + dI$. We assume that the spatial distribution of the laser intensity is Lorentzian in the propagation direction (z) and Gaussian in the transverse direction (ρ) [17,18]: namely,

$$I(\rho, z) = \frac{I_0 w_0^2}{w(z)^2} e^{-2\rho^2/w(z)^2},$$

with
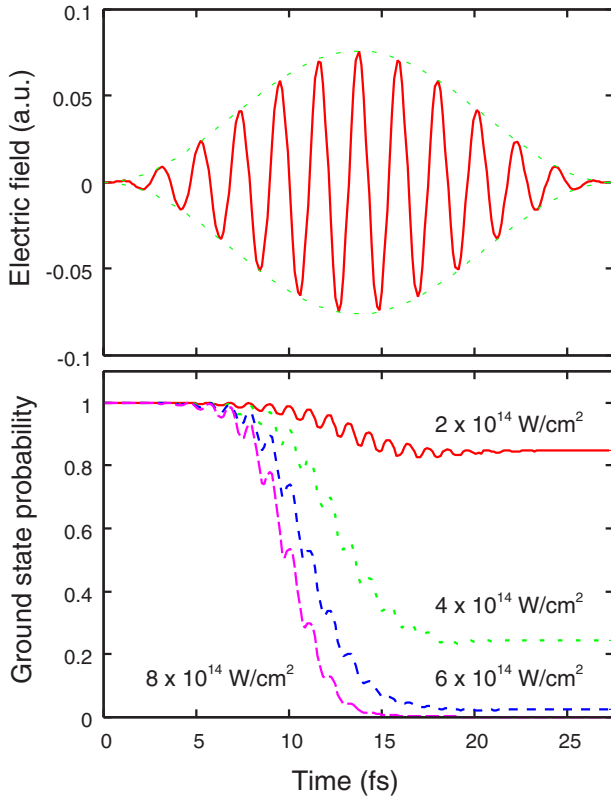
FIG. 2. (Color online) (Top) Time dependence of the electric field of a 640-nm 10-fs laser pulse with peak intensity of 8×10^{14} W/cm². (Bottom) Time evolution of the ground-state probabilities at the intensities indicated.

$$w(z) = w_0 \sqrt{1 + (z/z_R)^2},$$

where w_0 is the $1/e$ radius of the focal spot and z_R is the Rayleigh range of the focus. The volume element for this laser beam is given as

$$-\frac{\partial V}{\partial I} dI = \frac{\pi w_0^2 z_0}{3} \frac{1}{I} \left(\frac{I_0}{I} + 2 \right) \sqrt{\frac{I_0}{I} - 1} \, dI.$$

We use the trapezoidal rule for the integration over intensity with sufficiently small step size for the laser parameters used.

We now return to the experimental data shown in Fig. 1. The experiment was carried out with a laser pulse of the duration of about 40 fs and mean wavelength of 640 nm. In the calculation, we used a 10-fs pulse and then scaled the electron spectra by the ratio of the total ionization yield of a 40-fs pulse to that of a 10-fs pulse in the volume integration in Eq. (1). In this scaling the total ionization yield is calculated using the static field ionization rates in Ref. [19] for each intensity.

In Figs. 1(d)–1(f) we show the theoretical electron spectra for the three peak intensities indicated. The theoretical spectra for the two higher intensities look very similar. Likewise, the experimental spectra at these two intensities are almost identical. Note that the experimental data shown here are identical to Fig. 5 of Maharjan *et al.* [12] but have been replotted here with the same scaling and color coding as the theoretical results. Each spectrum is normalized at the maxi-
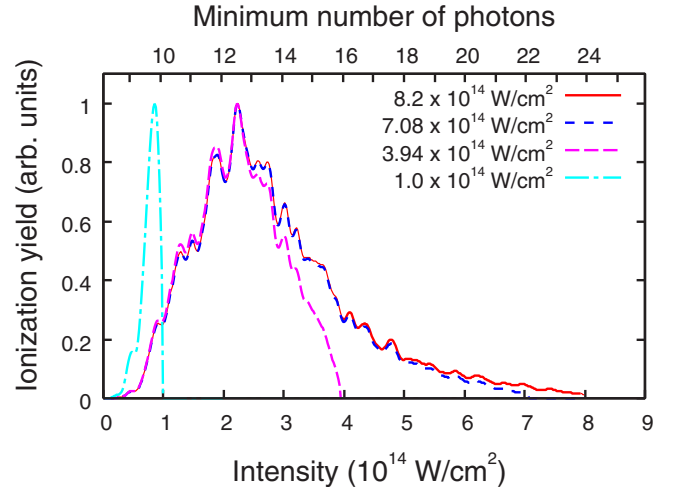
FIG. 3. (Color online) Differential intensity dependence of the low-energy part of the ionization yield ($\leqslant \hbar \omega$) multiplied by the volume element for a 640-nm 40-fs laser pulse with different peak intensities. Minimum number of photons needed to ionize the atom is indicated on the upper horizontal axis.

mum value and plotted in log scale. For yields that are less than $1/20$ of the maximum, the data were truncated. The agreement between the theory and experiment for the two higher intensities looks quite reasonable. At the lower peak intensity of 3.94×10^{14} W/cm², the agreement between theory and experiment is not as good where the theory predicts more high-energy electrons. We found that by substantially lowering the peak intensity to 1.0×10^{14} W/cm², the calculated electron images are closer to the measured spectra; see Fig. 1(g). Note that the experimentalists deduced the peak intensities by measuring the laser power, pulse length, and shape of the laser beam in the far-field region before the focusing mirror and estimated that the peak intensity is probably accurate to within about 30%.

Let us analyze the results of the theoretical calculations. In Fig. 3 we show the differential intensity contributions to the calculated electron spectra for each peak intensity, including the volume element, but only for the low-energy part where the electron energy is less than one photon energy, corresponding to momentum less than 0.37 a.u. It is interesting to see that the differential intensity contributions to the ionization yields for the two higher peak intensities, 8.2 and 7.08×10^{14} W/cm², are essentially exactly identical. Furthermore, in both cases, major contributions to the ionization yields come from intensities around 2×10^{14} W/cm², where $\gamma \sim 1$. Because of the depletion of the ground state, for these two pulses the intensity near the peak has few contributions to the ionization yield. Thus while two different peak intensities were used, as far as single ionization of the Ar atoms is concerned, the two pulses are identical and this explains why the two spectra in Figs. 1(a) and 1(b) are so similar. In fact, even at a peak intensity of 3.94×10^{14} W/cm², the main differential intensity region contributing to the total yield is also about the same. This explains why the calculated spectra at 3.94×10^{14} W/cm² shown in Fig. 1(f) are nearly identical to the ones shown in Figs. 1(d) and 1(e). In Fig. 3 we also show that at a peak intensity of 1.0×10^{14} W/cm², the volume
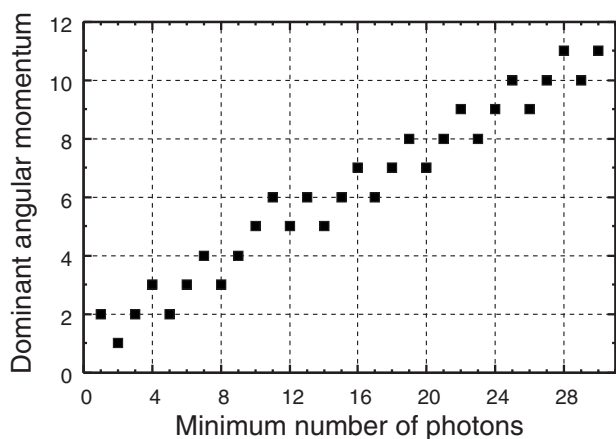
FIG. 4. The dominant angular momentum for low-energy ATI electrons vs the minimum number of photons needed to ionize an atom from an initial *p* orbital. Taken from Ref. [16].

effect becomes not significant and the measured electron spectra can be approximately attributed to a single peak field strength.

On the upper horizontal axis of Fig. 3, we also indicate the minimum number of photons, *N*, that have to be absorbed for the electron to be ionized, calculated using $N=(I_p+U_p)/(\hbar\omega)$, where ω is the angular frequency of the laser. I_p is the ionization potential and U_p is the ponderomotive energy, as described earlier. In a previous study [14,16], it was shown that when the low-energy electron momentum distributions have stripes fanning out radially from $p=0$, these electrons tend to be dominated by a single angular momentum. In Fig. 8 of Chen *et al.* [16] the relation between *N* and the dominant angular momentum for the low-energy electron has been empirically established. For completeness we reproduce the figure for atoms initially in the *p* state in Fig. 4. From Fig. 3, for the peak intensities of 8.2 and 7.08×10^{14} W/cm², most contributions come from the range of $(1-3)\times10^{14}$ W/cm², corresponding to *N* between 11 and 15. From Fig. 4, we read that the dominant angular momentum is 6 for *N*=11, 13, 15, and 5 for *N*=12, 14. If the angular momentum is taken to be 6, seven stripes fanning out from the center will be expected. That appears to be the case for momentum around 0.2. For lower momenta, the calculations show six stripes, which would correspond to angular mo-

mentum equal to 5; see Figs. 1(d) and 1(e). Thus the calculated results are in accordance with the model prediction of Fig. 4. In the experimental data, only five stripes can be clearly identified. Since the positions of the four stripes near the parallel direction in the experimental data agree with those in the theoretical ones, we tend to think that the two stripes near the perpendicular direction are blurred, possibly from contributions due to double ionization or from the different laser parameters used in the calculations and experiments.

The analysis of the previous paragraph also explains why the fanlike stripes at low electron energies survive the volume integration. These structures have been shown in Chen *et al.* [16] to be the ubiquitous features of low-energy electrons that see the long-range Coulomb potential of the core ion. The number of fans changes slowly with the laser intensity (or the minimum number of photons absorbed), such that volume integration does not smooth out these structures.

Another feature of the momentum images is the appearance of broken circular rings with constant values of momentum $p\sim0.3$ a.u.—these are Freeman resonances [2]. They occur only at specific laser intensities—when the energy position of a Rydberg state shifted by the ac Stark effect is equal to an integer multiple of the photon energy. For low laser intensities and long pulses the Freeman resonances are the dominant features in the spectra and have been extensively studied in the past [3]. For higher peak intensities, because of the focus volume integration in which a continuous range of laser intensity is covered, Freeman resonances are easily observed experimentally. In theoretical calculations like the present one, the chosen intensities are in discrete steps. Thus one has to be careful to make sure that the intensities where Freeman resonances occur are included in the calculation. We comment that the normal ATI peaks shift with laser's Ponderomotive energy which is proportional to laser intensity. These ATI peaks are smeared out after the volume integration and are not observed experimentally.

In Fig. 5 we compare the electron momentum spectra measured for a 40-fs 400-nm laser pulse with peak intensity of 1.4×10^{15} W/cm² and an 800-nm 25-fs pulse with intensity of 1.94×10^{14} W/cm² with our theoretical calculations. The experimental data are from Figs. 2 and 3 of Maharjan *et al.* [12], but replotted with the same color coding as the theoretically calculated ones. In the calculation we used a 10-fs pulse for the 400-nm case and a 20-fs pulse for 800-nm
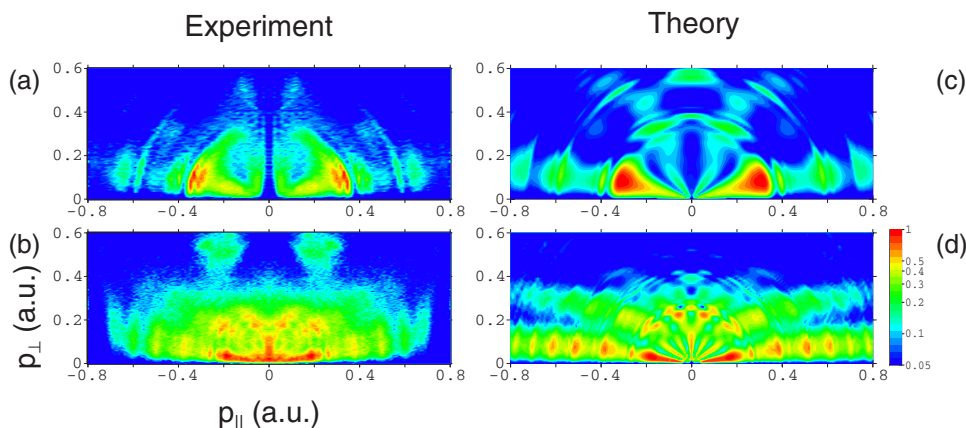
FIG. 5. (Color online) Comparison of theoretical and experimental electron momentum distributions of Ar by [(a) and (c)] a 400-nm 40-fs laser pulse with peak intensity of 1.4×10^{15} W/cm² and [(b) and (d)] an 800-nm 25-fs laser pulse with peak intensity of 1.94×10^{14} W/cm².
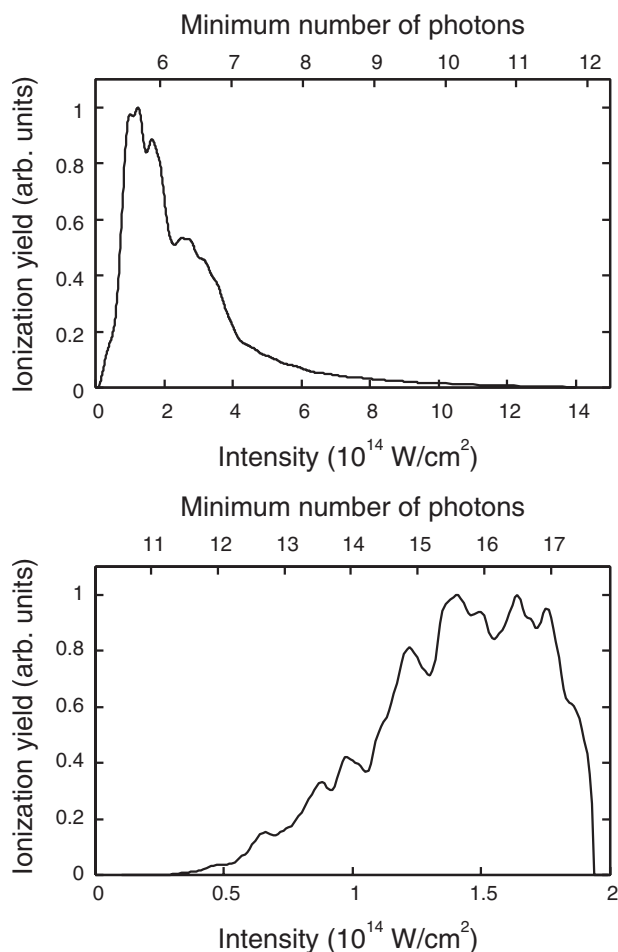
FIG. 6. Differential intensity dependence of the low-energy part of the ionization yield ($\leq \hbar\omega$) multiplied by the volume element for a 400-nm 40-fs laser pulse with peak intensity of 1.4×10^{15} W/cm^2 (top) and for a 800-nm 25-fs laser pulse with peak intensity of 1.94×10^{14} W/cm^2 (bottom). Minimum number of photons needed to ionize the atom is indicated on the upper horizontal axis of each frame.

case. The laser-focus volume effect was treated as in the 640-nm case shown in Fig. 1.

In Fig. 6 we show the differential intensity contributions to the total electron yield for electrons with energy less than $\hbar\omega$. Clearly for the 400-nm pulse with peak intensity of 1.4×10^{15} W/cm^2, most of the contributions to the electron images come from intensities near 2×10^{14} W/cm^2, where $\gamma \sim 1.6$. In this case, according to the upper horizontal labeling of Fig. 6, it would take six photons to ionize Ar at the intensity of 2×10^{14} W/cm^2. According to Fig. 4, the dominant angular momentum of the ejected electron is 3, and thus we expect four radial stripes. This is consistent with the theoretical calculations. The experimental data do not disagree with this statement even though the features of the fans away from the horizontal axis is not as clean. The theory predicts no electrons coming out at $p_\parallel=0$ for small p. Note that the vertical line at $p_\parallel=0$ in the experimental data is due to the instrumental arrangement of the detector, not the signal.

For the 800-nm case, the bottom figure shows that contributions to the electron momentum spectra come mostly from

laser intensities of $(1-1.8) \times 10^{14}$ W/cm^2, where γ is 1.4–0.8. It will take 15–17 photons to ionize Ar at these intensities. According to Fig. 4, the dominant angular momenta for these minimum numbers of photons are 6 and 7. The theoretical electron spectra show seven radial stripes fanning out from $p_\parallel=0$, favoring a dominant angular momentum of 6. In the experiment, the fanlike structures are less clear. However, we do see good overall agreement in the positions of the stripes close to the $p_\parallel$ axis and good agreement in other main features.

Based on the present analysis, let us comment on the earlier experimental data of Rudenko *et al.* [11] where longitudinal momentum distributions of the recoil ions have been measured; see Fig. 1 of that paper. For an Ar target, they reported experimental data for peak laser intensities from 1.5×10^{14} to 1.5×10^{15} W/cm^2. By analyzing the volume effect similar to those shown in Figs. 3 and 6, using the static field ionization rates, we found that the data for peak intensities from 5×10^{14} to 1.5×10^{15} W/cm^2 are essentially identical with the peak contribution from 3×10^{14} W/cm^2, where $\gamma \sim 0.7$ (i.e., almost like the two top intensities in Fig. 3). Thus the peak intensity dependence has no meaning and this also explains why the spectra look so similar in the experiment. At peak intensity of 1.5×10^{15} W/cm^2, their data are similar to the projection of the two-dimensional spectra of Fig. 5(b) on the longitudinal axis. For Ne atoms, due to its higher ionization potential, the depletion effect does not become important until at a higher intensity. According to our analysis, the effect of depletion makes the two highest intensities, 2.0×10^{15} and 1.5×10^{15} W/cm^2, result in identical differential intensity dependences. A close examination of their data showed indeed that the longitudinal momentum distributions of these two peak intensities are very similar. At peak intensities of 1.0×10^{15}, 6×10^{14}, and 4×10^{14} W/cm^2, we found that the dominant differential intensity that contributes to the volume integration occurs at 8×10^{14}, 5×10^{14}, and 3×10^{14} W/cm^2 or with a minimum of 44, 34, and 28 photons to ionize the neon atom, respectively. A similar analysis for He shows that it is closer to Ne, but at 1.5×10^{15} and 2.0×10^{15} W/cm^2, the differential intensity contributions to the electron spectra are different, because He has even higher ionization energy.

III. CONCLUSION

We have examined theoretically the laser-focus volume effect on the two-dimensional electron momentum spectra of single ionization of Ar atoms in the tunneling ionization regimes. At high peak laser intensities the Ar atom can be completely singly ionized before the laser pulse is over or before the peak intensity is reached. For highly focused laser beams, electrons are collected from regions where the laser intensities are much smaller than the peak intensity. Together with the fact that the electron spectra vary rapidly with laser intensities in general, comparison of experimental electron spectra with theoretical calculations cannot be made unless the volume effects are considered. For single ionization of atoms, we have shown two features in the two-dimensional electron momentum spectra. One is the well-known Freeman

resonances. These show more clearly in the electron energy spectra or in the longitudinal momentum spectra and only in longer pulses. The other features are the radial stripes fanning out from the zero momentum. These radial stripes are characterized by a dominant angular momentum over a range of laser intensities. The dominant angular momentum or the number of stripes changes slowly with the laser intensities. This slow variation makes it possible to survive the volume integration, and they are the main features of the two-dimensional low-energy electron momentum spectra, as observed in Rudenko *et al.* [11] and in Maharjan *et al.* [12]. On the other hand, as we have shown here, these experimental data cannot be compared to theoretical calculations with a given peak laser intensity, as has been done in previous attempts in the interpretation of these experimental data.

APPENDIX: TIME-DEPENDENT SCHRÖDINGER EQUATION SOLUTION

In this appendix we describe the method used in the solution of the time-dependent Schrödinger equation of a one-electron atom in a linearly polarized laser field which has been used to calculate the two-dimensional electron spectra. Our method differs somewhat from what exists in the literature.

We consider single ionization of $Ar(3p_0)$ by intense short laser pulses. For the laser parameters used, we expect the contribution from the $3p_{\pm 1}$ states to the electron spectra to be negligible. Within the single active electron approximation, the time-dependent Schrödinger equation for an atom in the presence of a linearly polarized laser field, in the length gauge, can be written as

$$i\frac{\partial}{\partial t}\Psi(\mathbf{r},t) = [H_0 + V(t)]\Psi(\mathbf{r},t), \quad (A1)$$

where

$$V(t) = E(t)z$$

is the time-dependent atom-laser interaction with $E(t)$ the time-dependent electric field chosen to be

$$E(t) = E\cos^2\left(\frac{\pi t}{\tau}\right)\cos(\omega t) \quad (A2)$$

for $-\tau \leq t \leq \tau$ and zero elsewhere. Here E is the amplitude of the electric field and the laser intensity is given by $I = \frac{1}{2}\epsilon_0 c E^2$. In Eq. (A1),

$$H_0 = -\frac{1}{2}\nabla^2 + \mathcal{L} + v(r) \quad (A3)$$

represents the target atomic Hamiltonian with $v(r)$ being the effective potential between the active electron and the core ion [19]. The Bloch operator,

$$\mathcal{L} = \frac{1}{2}\delta(r - r_M)\frac{\partial}{\partial r}$$

is introduced to make the kinetic operator Hermitian in the finite range of $r = [0, r_M]$. We solve the time-dependent equation by using a second-order split operator method,

$$\Psi(t + \Delta t) = e^{-iH_0\Delta t/2}e^{-iV(t+\Delta t/2)\Delta t}e^{-iH_0\Delta t/2}\Psi(t), \quad (A4)$$

expanding the wave function by the direct products of discrete variable representation (DVR) basis sets [20] associated with Legendre polynomials in both r and $\hat{z} = \cos\theta$ coordinates. We use the eigenvalues and eigenfunctions of H_0 to evaluate the matrix elements for the exponents in Eq. (A4). The probability for transition to a final ionizing state of the target with momentum $\mathbf{p}$ is then extracted by projecting onto the momentum-normalized continuum states with the incoming wave boundary condition $\psi_{\mathbf{p}}^{(-)}$,

$$P(\mathbf{p}) = \left|\lim_{t\to\infty}\int_{r\leq r_M}\Psi^*(t)\psi_{\mathbf{p}}^{(-)}d\mathbf{r}\right|^2. \quad (A5)$$

We calculate the continuum state wave function $\psi_{\mathbf{p}}$ for $r \leq r_M$ by using the Green's function G [21],

$$\psi_{\mathbf{p}}(\mathbf{r}) = \int_{r\leq r_M}G(\mathbf{r},\mathbf{r}')\mathcal{L}\psi_{\mathbf{p}}(\mathbf{r}')d\mathbf{r}',$$

where the Green function is obtained by the spectral resolution as

$$G(\mathbf{r},\mathbf{r}') = \sum_\gamma\frac{\varphi_\gamma(\mathbf{r})\varphi_\gamma(\mathbf{r}')}{\epsilon_\gamma - \epsilon}.$$

Here ϵ_γ and φ_γ are the eigenvalue and the associated eigenfunction of the Hamiltonian in the range of $[0, r_M]$ in Eq. (A3), respectively, and $\epsilon = \frac{p^2}{2}$ represents the ejected electron energy. The incoming wave boundary condition is incorporated into the wave function by matching to the continuum Coulomb wavefunctions at $r = r_M$ through the R matrix [21], obtaining the S matrix for the active electron and the core ion. In this procedure, integrations over the spatial coordinates, including the calculations of the matrix elements for the exponents in Eq. (A4) and the projection in Eq. (A5), are evaluated by using DVR quadratures efficiently. Similar time propagation-projection scheme was used in Ref. [22].

[1] L. V. Keldysh, Zh. Eksp. Teor. Fiz. **47**, 1945 (1964); Sov. Phys. JETP **20**, 1307 (1965).

[2] R. R. Freeman, P. H. Bucksbaum, H. Milchberg, S. Darack, D. Schumacher, and M. E. Geusic, Phys. Rev. Lett. **59**, 1092 (1987).

[3] R. Wiehle, B. Witzel, H. Helm, and E. Cormier, Phys. Rev. A **67**, 063405 (2003).

[4] P. Agostini, P. Breger, A. L'Huillier, H. G. Muller, G. Petite, A. Antonetti, and A. Migus, Phys. Rev. Lett. **63**, 2208 (1989).

[5] P. Hansch, M. A. Walker, and L. D. Van Woerkom, Phys. Rev. A **55**, R2535 (1997).

[6] H. G. Muller and F. C. Kooiman, Phys. Rev. Lett. **81**, 1207 (1998).

[7] R. Moshammer, J. Ullrich, B. Feuerstein, D. Fischer, A. Dorn, C. D. Schröter, J. R. Crespo Lopez-Urrutia, C. Hoehr, H. Rottke, C. Trump, M. Wittmann, G. Korn, and W. Sandner, Phys. Rev. Lett. **91**, 113002 (2003).

[8] J. Chen and C. H. Nam, Phys. Rev. A **66**, 053415 (2002).

[9] K. I. Dimitriou, D. G. Arbó, S. Yoshida, E. Persson, and J. Burgdörfer, Phys. Rev. A **70**, 061401(R) (2004).

[10] F. H. M. Faisal and G. Schlegel, J. Phys. B **38**, L223 (2005).

[11] A. Rudenko, K. Zrost, C. D. Schröter, V. L. B. de Jesus, B. Feuerstein, R. Moshammer, and J. Ullrich, J. Phys. B **37**, L407 (2004).

[12] C. M. Maharjan, A. S. Alnaser, I. Litvinyuk, P. Ranitovic, and C. L. Cocke, J. Phys. B **39**, 1955 (2006).

[13] A. S. Alnaser, C. M. Maharjan, P. Wang, and I. V. Litvinyuk, J. Phys. B **39**, L323 (2006).

[14] D. G. Arbó, S. Yoshida, E. Persson, K. I. Dimitriou, and J. Burgdörfer, Phys. Rev. Lett. **96**, 143003 (2006).

[15] M. Wickenhauser, X. M. Tong, D. G. Arbó, J. Burgdörfer, and C. D. Lin, Phys. Rev. A **74**, 041402(R) (2006).

[16] Z. Chen, T. Morishita, A.-T. Le, M. Wickenhauser, X.-M. Tong, and C. D. Lin, Phys. Rev. A **74**, 053405 (2006).

[17] A. E. Siegman, *Lasers* (University Science Books, Sausalito, CA, 1986).

[18] S. Augst, D. D. Meyerhofer, D. Strickland, and S. L. Chin, J. Opt. Soc. Am. B **8**, 858 (1991).

[19] X. M. Tong and C. D. Lin, J. Phys. B **38**, 2593 (2005).

[20] D. O. Harris, G. G. Engerholm, and W. D. Gwinn, J. Chem. Phys. **43**, 1515 (1965); A. S. Dickinson and P. R. Certain, *ibid.* **49**, 4209 (1968); J. C. Light and R. B. Walker, *ibid.* **65**, 4272 (1976).

[21] K. L. Baluja, P. G. Burke, and L. A. Morgan, Comput. Phys. Commun. **27**, 299 (1982).

[22] T. Morishita, K. Hino, T. Edamura, D. Kato, S. Watanabe, and M. Matsuzawa, J. Phys. B **34**, L475 (2001); T. Morishita, T. Sasajima, S. Watanabe, and M. Matsuzawa, Nucl. Instrum. Methods Phys. Res. B **214**, 144 (2004).